A&A 381, 1007–1014 (2002)
DOI: 10.1051/0004-6361:20011535

Astronomy & Astrophysics

Spectral analysis of the sdO K 648, the exciting star of the planetary nebula Ps 1 in the globular cluster M 15 (NGC 7078)⋆

T. Rauch[1], U. Heber[2,⋆⋆], and K. Werner[1]

[1] Institut für Astronomie und Astrophysik, Universität Tübingen, 72076 Tübingen, Germany
[2] Dr. Remeis-Sternwarte, Universität Erlangen-Nürnberg, 96049 Bamberg, Germany

Received 17 July 2001 / Accepted 29 October 2001

Abstract. We present a spectral analysis of the sdO central star K 648 based on medium-resolution optical and high-resolution UV spectra. The photospheric parameters are determined by means of state-of-the-art NLTE model atmosphere techniques. We found $T_{\rm eff} = 39 \pm 2$ kK and $\log g = 3.9 \pm 0.2$. The helium ($n_{\rm He}/n_{\rm H} = 0.08$) and oxygen ($n_{\rm O}/n_{\rm H} = 0.001$) abundances are about solar while carbon is enriched by a factor of 2.5 ($n_{\rm C}/n_{\rm H} = 0.001$). Nitrogen ($n_{\rm N}/n_{\rm H} = 1 \times 10^{-6}$, [N/H] = −2.0) appears at a sub-solar value. However, these metal abundances are much higher than the cluster's metallicity (M 15: [Fe/H] = −2.25). The surface composition appears to be a mixture of the original hydrogen-rich material and products of helium burning (3α process) which have been mixed up to the surface. The abundances of He, C, and N are consistent with the nebular abundance, while O is considerably more abundant in the photosphere than in the nebula. From a comparison of its position in the $\log T_{\rm eff}$–$\log g$ plane with evolutionary calculations a mass of $0.57^{+0.02}_{-0.01}\,M_\odot$ and a luminosity of $3810 \pm 1200\,L_\odot$ are deduced. Our spectroscopic distance $d = 11.1^{+2.4}_{-2.9}$ kpc is in agreement with the distance of M 15 as determined by Alves et al. (2000). From the GHRS spectra we measure a radial velocity of $v_{\rm rad} = -130\,{\rm km\,s^{-1}}$.

Key words. Galaxy: globular clusters: individual: M 15 – ISM: planetary nebulae: individual: Ps 1 – stars: abundances – stars: AGB and post-AGB – stars: evolution – stars: individual: K 648

1. Introduction

K 648 ($m_V = 14.73$, Alves et al. 2000) was registered by Küstner (1921) close to the center ($\Delta\alpha = +14''$, $\Delta\delta = +26''$) of the galactic globular cluster M 15. A spectrum taken by Pease (1928) shows a continuous O-type spectrum and characteristic emission lines of a planetary nebula (Ps 1, PN G065.0-27.3). Pease derived a radial velocity of $v_{\rm rad} = -180 \pm 50$ km s^{-1} from his spectrum and concluded that K 648 is probably the first PN discovered in a globular cluster.

Joy (1949) improved the radial-velocity measurement ($v_{\rm rad} = -115$ km s^{-1}) and concluded that, without doubt, Ps 1 is a member of M 15 ($v_{\rm rad} = -107$ km s^{-1}, Harris 1996) because of the close agreement of their radial velocities.

The existence of a PN in M 15 is unexpected: at a turn-off age of 12 billion years, the most massive main-sequence stars in M 15 should have $M_{\rm initial} \lesssim 0.8\,M_\odot$. For such low-mass stars it is almost impossible to ascend to the AGB and eject a PN. An analysis of the nebula properties by Adams et al. (1984) yields a solar He/H ratio and a slightly higher than solar C/H ratio while the total N, O, and Ne abundance is less than solar by a factor of 18 (Fig. 13). The high carbon abundance in the PN was interpreted by Adams et al. as a product of helium burning (3α process) and a subsequent third dredge-up which has brought the material to the stellar surface. The nebula ejection has taken place then after this event.

Alves et al. (2000) suggest that the progenitor of K 648 experienced mass augmentation in a close binary merger and thus, the remnant has a higher mass than remnants of single stars in M 15.

A preliminary analysis of the optical and GHRS spectra (Table 1) by means of line-blanketed NLTE model atmosphere techniques by Heber et al. (1993) revealed

Send offprint requests to: T. Rauch,
e-mail: rauch@astro.uni-tuebingen.de

⋆ Based on observations obtained at the German-Spanish Astronomical Center, Calar Alto, operated by the Max-Planck-Institut für Astronomie Heidelberg jointly with the Spanish National Commission for Astronomy, on data retrieved from the International Ultraviolet Explorer (IUE) Final Archive, on observations made with the Hubble Space Telescope (HST, GO Proposal ID: 3513, PI: Heber), and on HST data retrieved from the ST-ECF archive.

⋆⋆ Visiting astronomer, Calar Alto, Spain.

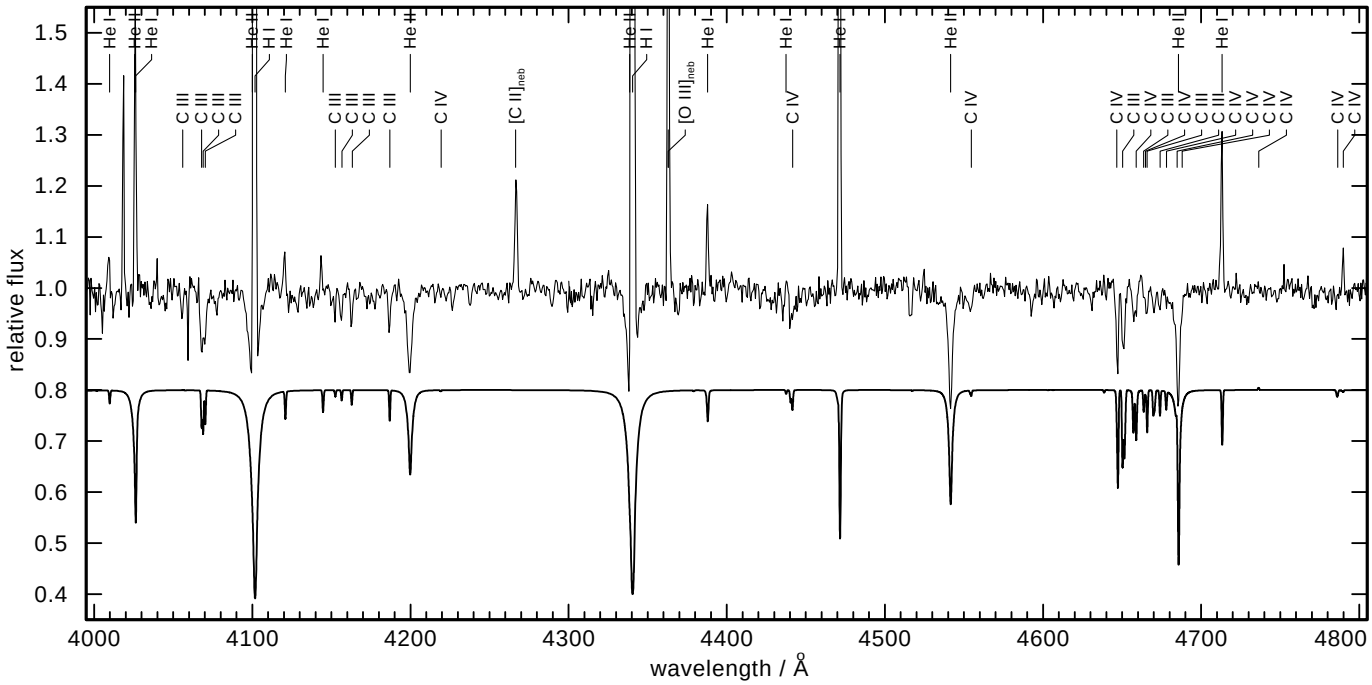

Fig. 1. Optical spectrum of K 648 obtained with the TWIN spectrograph (top). Positions of H I, He I-II, and C III-IV lines are indicated. Note the contamination by nebula emission, e.g. around H γ and He I λ 4471 Å. A synthetic spectrum (parameters from Table 2) is shown at the bottom.

$T_{\rm eff} = 37$ kK, $\log g = 4.0$, $n_{\rm He}/n_{\rm H} = 0.5$ (by number) and a three times solar carbon abundance. Since this is much higher than the metallicity of M 15 an explanation for the evolutionary history of K 648 and its PN is difficult. Bianchi et al. (1995, see this paper for a more detailed introduction) presented a first analysis of HST data and arrived at $T_{\rm eff} = 35$ kK. Another spectral analysis based on high-resolution Keck spectra was presented by McCarthy et al. (1997). They arrived at $T_{\rm eff} = 43$ kK, $\log g = 3.9$, $n_{\rm He}/n_{\rm H} = 0.08$ and a solar carbon abundance. However, in contrast to Heber et al. (1993), NLTE line blanketing had not been taken in account in these models.

Recently a LTE abundance analysis was presented by Bianchi et al. (2001): they used $T_{\rm eff}$ and $\log g$ from Heber et al. (1993) and arrived even at a two times higher helium abundance of $n_{\rm He}/n_{\rm H} = 0.6$, carbon is four times solar, oxygen underabundant, and silicon is about solar.

In order to investigate the enigma of K 648, we have performed a new NLTE spectral analysis based on state-of-the-art metal-line blanketed model atmospheres.

2. Observations

2.1. Ultraviolet spectra

The following spectral analysis is mainly based on HST "preview" spectra (Table 1) which were retrieved from the archive operated at ST-ECF.

The high-resolution GHRS spectra allow to measure the radial velocity of K 648 precisely: in Z1BN0106T and Z1BN0107T (Table 1) the photospheric lines are blueshifted by 0.55 and 0.57 Å (we used the C III C IV, N V, and O IV lines in the spectra to measure the shift) and hence $v_{\rm rad} = -128$ and $-133\,{\rm km\,s^{-1}}$, respectively. This is close to the values given by Joy (1949, -115 and $-129\,{\rm km\,s^{-1}}$) and Schneider et al. (1983, $-128\,{\rm km\,s^{-1}}$). However, the velocity of M 15 is somewhat smaller ($v_{\rm rad} = -107\,{\rm km\,s^{-1}}$, Harris 1996).

The analysis of UV spectra requires a careful determination of the stellar continuum. Thus we start already here with an investigation of the interstellar H I column density (Sect. 2.1.2) and the interstellar reddening (Sect. 2.1.2). The NLTE spectral analysis is then described in Sect. 3.

2.1.1. Interstellar sulfur lines

Two interstellar lines, S II $\lambda\lambda$ 1250.59, 1253.81 Å, are prominent in the GHRS spectra. This allows to measure the wavelength shift of the ISM: it is blueshifted by about 0.145 Å (this is equivalent to $v_{\rm rel} = -35\ {\rm km\,s^{-1}}$). This values allows e.g. to identify the interstellar contribution to the photospheric N V lines (Sect. 3.3).

2.1.2. Interstellar neutral hydrogen and reddening

A H I column density of $n_{\rm H\,I} = 5\ (\pm 1) \times 10^{20}\,{\rm cm^{-2}}$ is determined from the Ly α profile (Fig. 2). The interstellar reddening is then estimated by means of the relation $n_{\rm H\,I} = (3.8 \pm 0.9) \times 10^{21} E_{B-V}$ (Groenewegen & Lamers 1989) yielding a color excess of $E_{B-V} = 0.13^{+0.08}_{-0.04}$. We use this result to compare a synthetic spectrum (from a

Table 1. Summary of the archival HST spectra which are used in this analysis.

image #	instrument	grating	exposure time / s	wavelength range / Å	resolution / Å	date
Y1C40105T	FOS	G130H	1800	1153–1605	0.96	93–11–18
Y1C40106T	FOS	G130H	1800	1153–1605	0.96	93–11–18
Y1C40104T	FOS	G190H	900	1573–2330	1.41	93–11–18
Y1C40103P	FOS	G270H	600	2221–3300	2.01	93–11–18
Z1BN0106T	GHRS	G160M	3917	1223–1259	0.07	93–05–15
Z1BN0107T	GHRS	G160M	3699	1315–1351	0.07	93–05–15

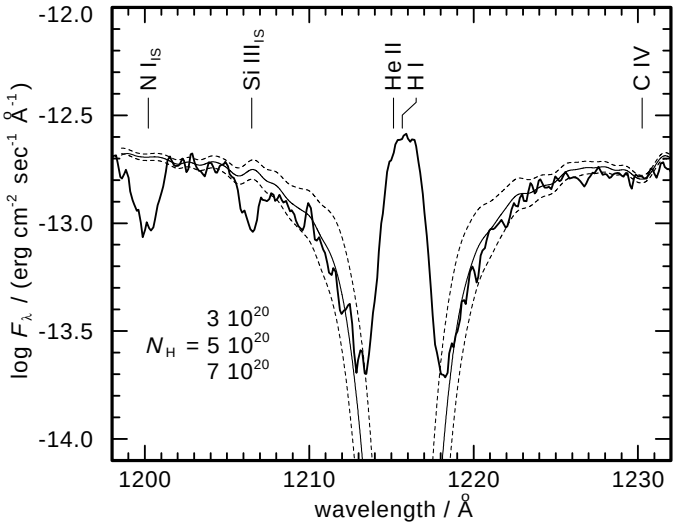

Fig. 2. Comparison of the theoretical Ly α profile with the FOS spectrum. The best fit is achieved at $n_{\rm H\,I} = 5 \times 10^{20}/{\rm cm}^2$. The theoretical flux is reddened according to $n_{\rm H\,I}$ (the continuum is scaled to fit the line wings of Ly α, Sect. 2.1.2). The parameters of the line-blanketed model atmosphere are summarized in Table 2.

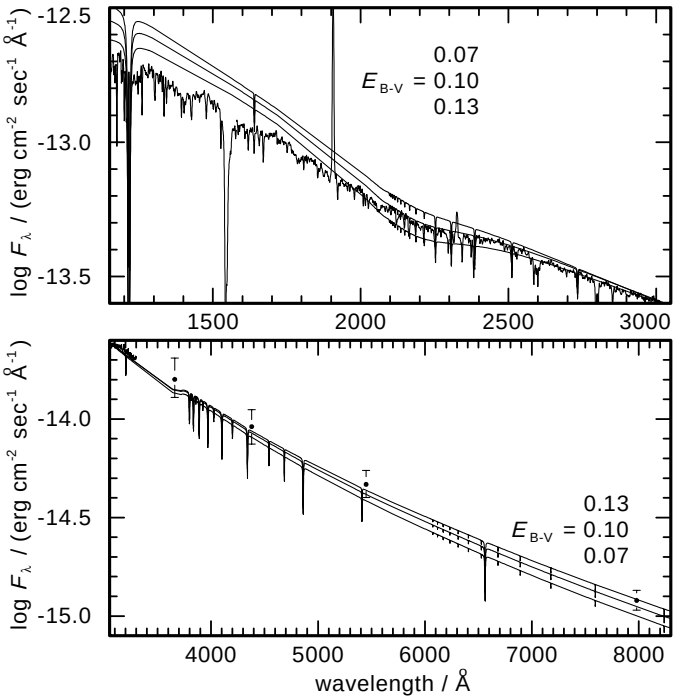

Fig. 3. Determination of the interstellar reddening. A synthetic spectrum, calculated from a H+He model ($T_{\rm eff} = 39$ kK, $\log g = 3.9$, $n_{\rm He}/n_{\rm H} = 0.08$), is shown with a reddening according to $E_{B-V} = 0.07$, 0.10, and 0.13. At longer wavelengths ($\lambda \gtrsim 2000$ Å) the observation is well fitted with $E_{B-V} = 0.10$ while at shorter wavelengths the reddening is underestimated. In the optical wavelength range (bottom), the measurements by Alves et al. (2000) are indicated with their error bars. The higher E_{B-V} seems to fit slightly better in the optical, however, then the fit to the measured UV flux is worse.

H+He model) with the FOS spectrum of K 648 (Fig. 3). In agreement with the above values, we achieve a good fit at $E_{B-V} = 0.10$ in the wavelength range 2100–3200 Å. This is also the amount of the foreground reddening towards M 15 (Harris 1996).

At shorter wavelengths the model predicts a higher flux level than observed. This discrepancy is not caused by metal-line blanketing. Even when we increase the abundances to solar, no match can be achieved (Fig. 4). Instead there a significantly different reddening law might be valid.

Since IUE spectra (e.g. SWP 17069) show the same flux level like the FOS spectra in the wavelength range around 1400 Å (not shown), problems in the flux calibration appear to be unlikely.

In the FOS spectra, we will use the He II Fowler series for our analysis (Fig. 5) which is located in the part of the spectrum that is well matched by the model. Thus we adopt $E_{B-V} = 0.10$ for our analysis. In the case of detailed line profile fits to the FOS and GHRS spectra, the model continuum has to be individually scaled in order to fit the observed continuum around the analyzed line.

2.2. Optical spectra

The optical spectra (resolution = 1 Å) of K 648 were obtained at the 3.5 m telescope at the Calar Alto (DSAZ, Spain) on June 12, 1989 with an exposure time of 2100 s. Since these spectra are, in contrast to the UV spectra which are used here, not absolutely calibrated we use the rectified spectrum (e.g. Fig. 1) instead.

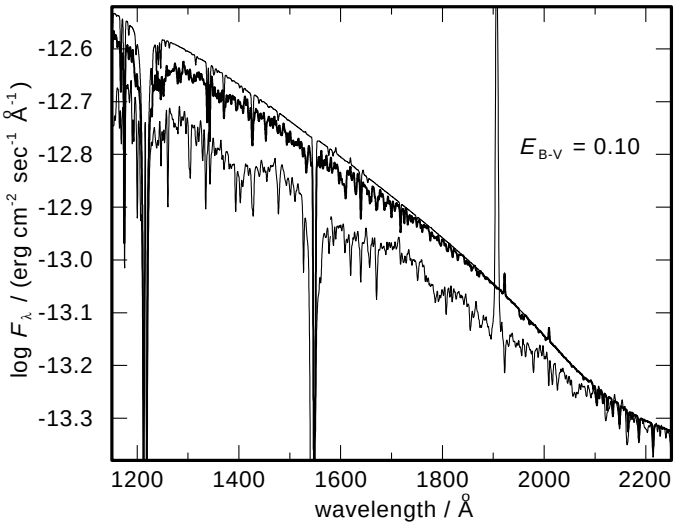

Fig. 4. Impact of iron-group opacities on the UV flux (model parameters: Table 2). Even at solar iron-group abundances (thick line), the model flux is much higher than observed. At the cluster metallicity [Fe/H] = −2.25, the iron-group opacities can be almost neglected (fine line). The synthetic spectrum is scaled to fit the observed flux at 3000 Å.

Since K 648 lies close to the center of M 15, the background determination was difficult (Heber et al. 1993) due to the low spatial resolution of the TWIN spectrograph.

Some of the "strategic" spectral lines are contaminated by nebular emission (Fig. 1) and thus unreliable: e.g. the He I / He II ionization equilibrium which is usually a very sensitive indicator for the effective temperature $T_{\rm eff}$ cannot be evaluated because all He I lines are filled in by nebular emission. However, He II lines as well as some carbon lines can be measured and will be used in our spectral analysis.

3. NLTE analysis

Bianchi et al. (1995) found evidence for a stellar wind of K 648 and derived $v_{\rm inf} = 1630$ km s^{-1} and $\log \dot{M}/(M_\odot\ {\rm yr}^{-1}) = -8.2$ from the strong C IV $\lambda\lambda$ 1548, 1550 Å resonance doublet. Other spectral lines appear unaffected by the wind. Hence, the plane-parallel, hydrostatic NLTE model atmospheres (Werner 1986; Rauch 1997; Rauch 2000, and references therein) are appropriate for this analysis.

In order to model the background opacity, metal-line blanketing of the iron-group elements (Dreizler & Werner 1993; Haas et al. 1996) is considered with a generic model atom. This is constructed from all elements Ca–Ni (ionization stages III–VII with all lines given by Kurucz 1996). Reduced abundances ([Z/H] = −2.25, following Harris 1996) are assumed. However, the impact of the Ca-Ni lines on the spectrum is small (Fig. 4).

In order to check the validity of the preliminary parameters from Heber et al. 1993 ($T_{\rm eff} = 37$ kK, $\log g = 4.0$, $n_{\rm He}/n_{\rm H} = 0.5$) we have performed some test calculations. From the comparison of synthetic spectra calculated from the new H+He models to the observation we find that g is in good agreement, while $T_{\rm eff}$ is higher and $n_{\rm He}/n_{\rm H}$ is about solar. The differences can be explained by the fact that our NLTE model atmospheres have been significantly improved since 1993 (e.g. Rauch 1997; Rauch 2000): the metal-line blanketing of all elements up to the iron group is considered in detail and thus the temperature structure is correctly modelled and subsequent line-formation calculations in order to determine metal abundances are much more reliable. E.g. the high He abundance found by Heber et al. (1993) and Bianchi et al. (2000) is due to artificial effects if model atoms are too small and/or metal-line blanketing is not accounted for in the model atmosphere calculation.

Due to the impact of CNO on the atmospheric structure and background opacity we decided to calculate a grid of H+He+C+N+O+(Ca-Ni) models in order to use e.g. the C III / C IV ionization equilibrium to determine $T_{\rm eff}$ reliably. The analysis is described in the following.

3.1. Surface gravity and helium abundance

The first parameter to be fixed is g. For this purpose we use two strongest uncontaminated lines in the optical spectrum, He II $\lambda\lambda$ 4200, 4541 Å (Fig. 1). We have calculated H+He models with $T_{\rm eff} = 37$−43 kK, $\log g = 3.5$−4.5 at different $n_{\rm He}/n_{\rm H}$ ratios. Although $T_{\rm eff}$ cannot reliably be judged from this approach, the $n_{\rm He}/n_{\rm H}$ is about solar. He II λ 4686 Å may be contaminated by nebular emission is not considered. Models with $\log g = 3.7$−4.2 and $n_{\rm He}/n_{\rm H} = 0.06$−0.10 (by number) fit the observation well (Fig. 6). These values are consistent with our more detailed models which account for metal-line blanketing (see below). We adopt $\log g = 3.9$ and $n_{\rm He}/n_{\rm H} = 0.08$. An error of 0.3 dex can be estimated by the variation of $T_{\rm eff}$ and $\log g$ within their error range and the quality of the available spectrum.

3.2. Effective temperature and carbon abundance

In the optical spectrum of K 648, the He I lines are contaminated by nebular emission, and thus, a commonly used tool to determine $T_{\rm eff}$, the He I / He II ionization equilibrium, cannot be used. The GHRS UV observations (Table 1) had been used with the aim to evaluate the C III / C IV ionization equilibrium (Heber et al. 1993) which is also a very sensitive indicator for $T_{\rm eff}$ (cf. Rauch 1993).

Since there are a lot of carbon lines identified in the optical spectrum (Fig. 1) we will use them to determine the carbon abundance first and then model the C III / C IV ionization equilibrium precisely. New H+He+C+N+O+(Ca–Ni) models ($T_{\rm eff} = 39$ kK, $\log g = 3.9$, $n_{\rm He}/n_{\rm H} = 0.08$, [(Ca–Ni)/H] = −2.25 have been calculated and the CNO abundances were

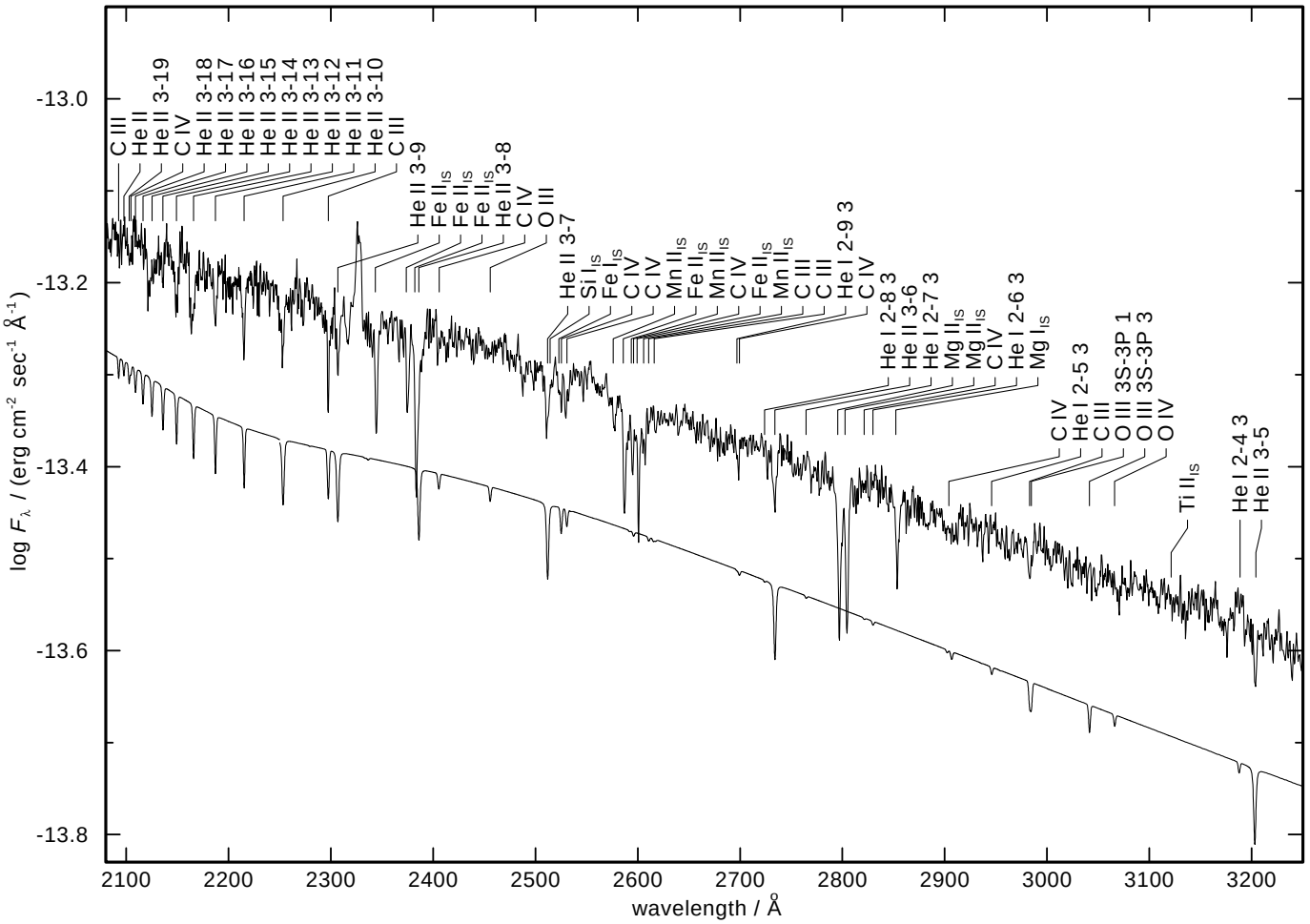

Fig. 5. UV spectrum of K 648 obtained with the FOS (top). Same like Fig. 1. Note that the He II lines, calculated with $n_{\rm He}/n_{\rm H} = 0.08$ are well matched.

adjusted to fit the observation (Fig. 7). We adopt $n_{\rm C}/n_{\rm H} = 0.001 \pm 0.3$ dex.

We calculated synthetic spectra from a small grid of models with $T_{\rm eff} = 37{-}43$ kK and $n_{\rm C}/n_{\rm H} = 0.001$. It turned out that the C III lines are strongly dependent on variation of $T_{\rm eff}$ while the C IV lines appear almost unchanged (Fig. 8). From the fit of the strongest C III line in the FOS spectrum of K 648, the C III λ 1175 Å triplet, we determine $T_{\rm eff} = 39 \pm 2$ kK (Fig. 8).

This result is verified by the C III and C IV lines in the high-resolution GHRS spectra (Fig. 9).

3.3. Photospheric nitrogen and oxygen abundances

In the last step, we determine the N and O abundances. New H+He+C+N+O+iron-group (Sect. 3) models are calculated. In the GHRS spectra, the most prominent N and O lines are the N V λ 1238, 1242 Å resonance doublet (apparently unaffected by the stellar wind (Sect. 3) and the O IV $\lambda\lambda$ 1338, 1343 Å lines. We use these in order to determine the abundances. We achieve $n_{\rm N}/n_{\rm H} = 1 \times 10^{-6}$ (Fig. 10) and $n_{\rm O}/n_{\rm H} = 1 \times 10^{-3}$ (Fig. 11). Due to the S/N ratio of the spectra, an error of ± 0.5 dex has to be assumed. Note that the line cores are much too strong at higher abundances.

4. Mass, luminosity, post-AGB age, and spectroscopic distance

In Fig. 12 we compare the position of K 648 with standard evolutionary tracks of hydrogen-burning post-AGB stars. From the evolutionary calculations of Schönberner (1983) we interpolate a stellar mass of $0.57^{+0.02}_{-0.01}\,M_\odot$, a luminosity of $3810 \pm 1200\,L_\odot$, and a post-AGB age of $6800^{+3\,500}_{-2\,100}$ a.

From our final model (Table 2), we can determine the spectroscopic distance of K 648 using the flux calibration of Heber et al. (1984):

$$f_V = 3.58 \times 10^{-9} \times 10^{-0.4 m_{V_0}} \,{\rm erg\,cm^{-2}\,s^{-1}\,\AA^{-1}} \qquad (1)$$

with $m_{V_0} = m_V - 2.175c$, $c = 1.47 E_{B-V} = 0.147$ (Fig. 3), $m_V = 14.73$, and $M = 0.57\ M_\odot$, the distance is derived from

$$d = 7.11 \times 10^4 \sqrt{H_\nu \cdot M \times 10^{0.4 m_{V_0} - \log g}}\ {\rm pc}\,. \qquad (2)$$

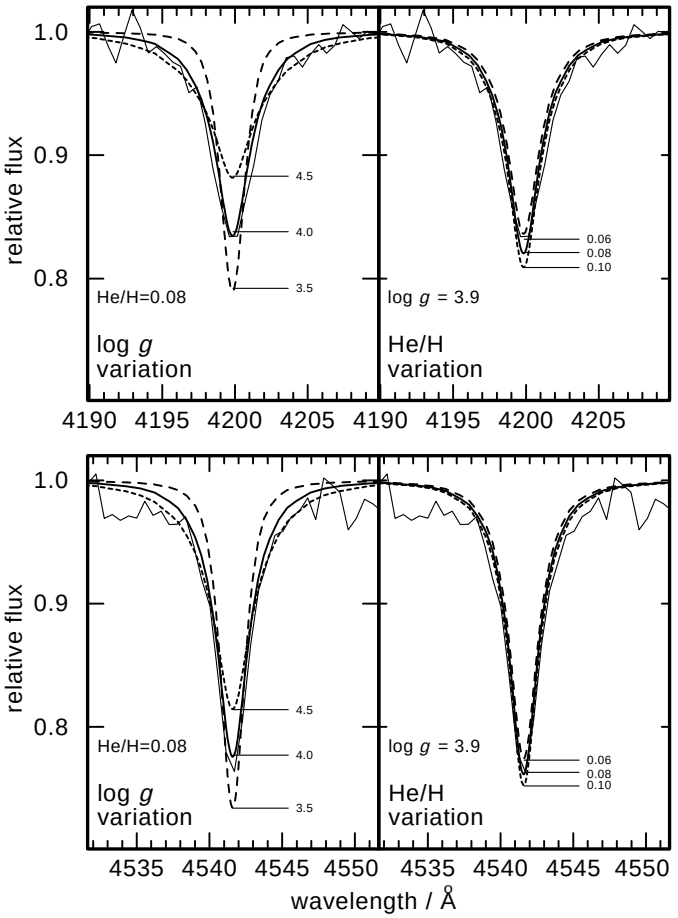

Fig. 6. Theoretical line profiles ($T_{\rm eff}=39$ kK, convolved with a Gaussian of 1 Å *FWMH* in order to match the instrumental resolution) of He II $\lambda\,4200$ Å (top) and He II $\lambda\,4541$ Å (bottom) compared with the observation. At $3.7 \lesssim \log g$ or $\log g \gtrsim 4.2$ no good fit can be achieved.

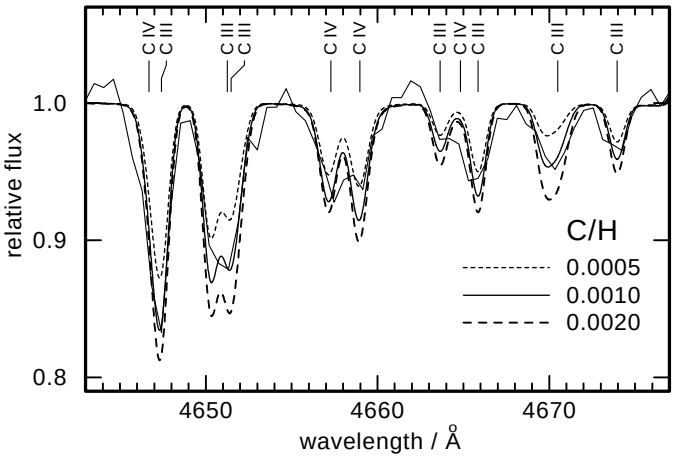

Fig. 7. Synthetic spectra from models with $T_{\rm eff}=39$ kK, $\log g=3.9$, $n_{\rm He}/n_{\rm H}=0.08$ and different $n_{\rm C}/n_{\rm H}$ ratios compared with the observation. At $n_{\rm C}/n_{\rm H}=0.0005$ (about solar ratio) all C lines appear too shallow. At $n_{\rm C}/n_{\rm H}=0.001$ the C III lines are still too weak while the C IV are already too strong. This indicates a slightly lower $T_{\rm eff}$. At higher $n_{\rm C}/n_{\rm H}$ ratios, no fit of the C lines is possible.

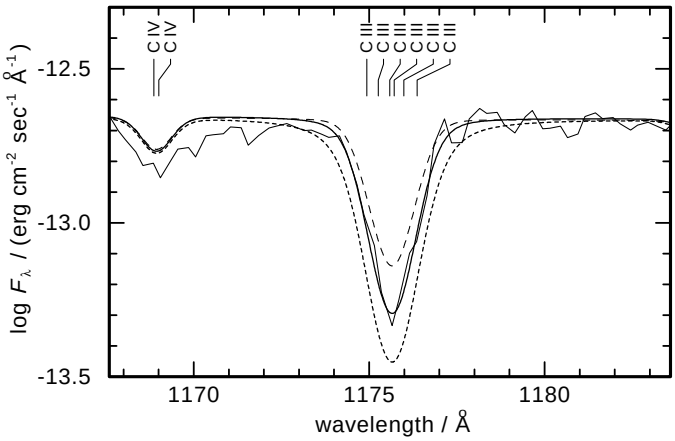

Fig. 8. Synthetic spectra with $T_{\rm eff}=37$ (short dashes), 39 (fully drawn), and 41 (long dashes) kK compared with the FOS spectrum (Table 1). At $T_{\rm eff}=39$ kK C III $\lambda\,1175$ Å is well matched.

With the Eddington flux at $\lambda_{\rm eff}=5454$ Å our final model atmosphere $H_\nu = 5.31\times10^{-4}\,{\rm erg\,cm^{-2}\,s^{-1}\,Hz^{-1}}$ we derive a distance of $d=11.1^{+2.4}_{-2.9}$ kpc. This distance is in agreement with the distance of the globular cluster M 15 ($d=12.3\pm0.6$ kpc, Alves et al. 2000).

5. The surrounding nebula Ps 1

For the ambient nebula, we can calculate the following: The linear dimension of the inner shell ($0\farcs8\times0\farcs6$, Alves et al. 2000) is $0.043^{+0.009}_{-0.011}\times0.032^{+0.007}_{-0.008}$ pc, and of the outer shell ($3\farcs1\times2\farcs7$, Alves et al. 2000) it is $0.166^{+0.035}_{-0.044}\times0.145^{+0.031}_{-0.038}$ pc. If we assume an average expansion velocity of $v_{\rm exp}=20\,{\rm km\,s^{-1}}$, then the dynamical age is $t_{\rm dyn}=3950^{+\,850}_{-1050}$ a. This is within the error range in agreement with its post-AGB age ($6800^{+3\,500}_{-2\,100}$ a, Sect. 4).

6. Results and discussion

In our analysis it became clear that the determination of $T_{\rm eff}$ from the two available GHRS spectra alone (C III / C IV ionization equilibrium) is not precise enough (too few lines to evaluate) – together with the available IUE, FOS, and TWIN spectra, however, we determined $T_{\rm eff}=39\pm2$ kK and $\log g=3.9\pm0.2$ which is within the error ranges in good agreement with the preliminary values given by Heber et al. (1993, 37 kK/4.0). In contrast to Heber et al., however, we arrive at an almost solar ($n_{\rm He}/n_{\rm H}=0.08$) He abundance. The high carbon abundance (2.5 times solar) is verified. The photospheric parameters of K 648 are summarized in Table 2.

The solar $n_{\rm He}/n_{\rm H}$ surface abundance indicates that K 648 might be a H-burning post-AGB star. Compared to the metallicity of M 15, the C and O abundances appear enriched (Fig. 13), likely due to a He-shell flash.

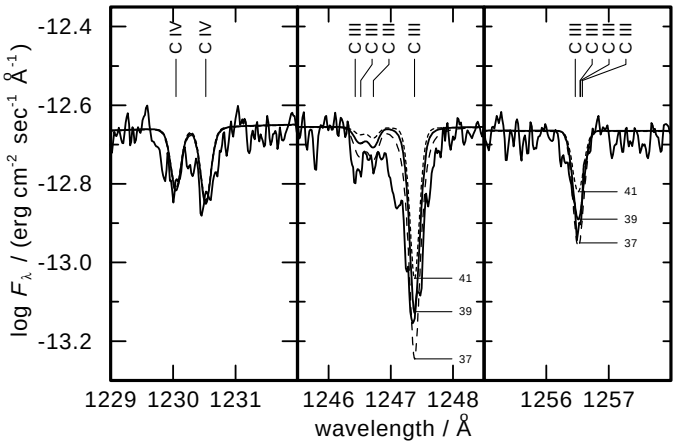

Fig. 9. Synthetic spectra with $T_{\rm eff}=$ 37 (long dashes), 39 (fully drawn), and 41 (short dashes) kK compared with the GHRS spectrum (Table 1). C III $\lambda\,1247$ Å is reproduced at $T_{\rm eff}=39$ kK, C III $\lambda\,1256$ Å at $T_{\rm eff}=38$ kK. C IV $\lambda\,1230$ Å is almost unchanged in this $T_{\rm eff}$ range.

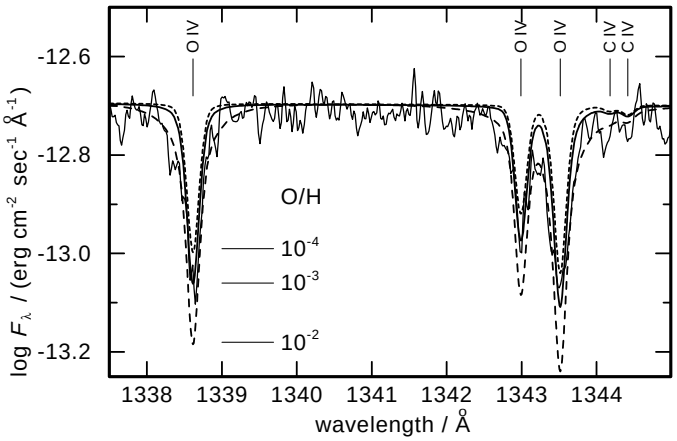

Fig. 11. Synthetic spectra with $T_{\rm eff}=39$ kK, $\log g=3.9$, $n_{\rm He}/n_{\rm H}=0.08$, $n_{\rm C}/n_{\rm H}=1\times10^{-3}$, $n_{\rm N}/n_{\rm H}=1\times10^{-5}$, and different O abundances compared with the GHRS spectrum (Table 1). O IV $\lambda\lambda\,1338, 1343$ Å is reproduced at $n_{\rm O}/n_{\rm H}=1\times10^{-3}$.

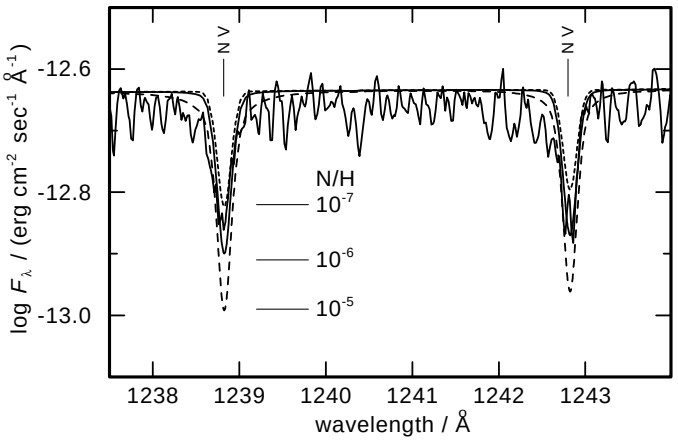

Fig. 10. Synthetic spectra with $T_{\rm eff}=39$ kK, $\log g=3.9$, $n_{\rm He}/n_{\rm H}=0.08$, $n_{\rm C}/n_{\rm H}=1\times10^{-3}$, $n_{\rm O}/n_{\rm H}=1\times10^{-3}$, and different N compared with the GHRS spectrum (Table 1). N V $\lambda\,1238, 1242$ Å is reproduced at $n_{\rm N}/n_{\rm H}=1\times10^{-6}$.

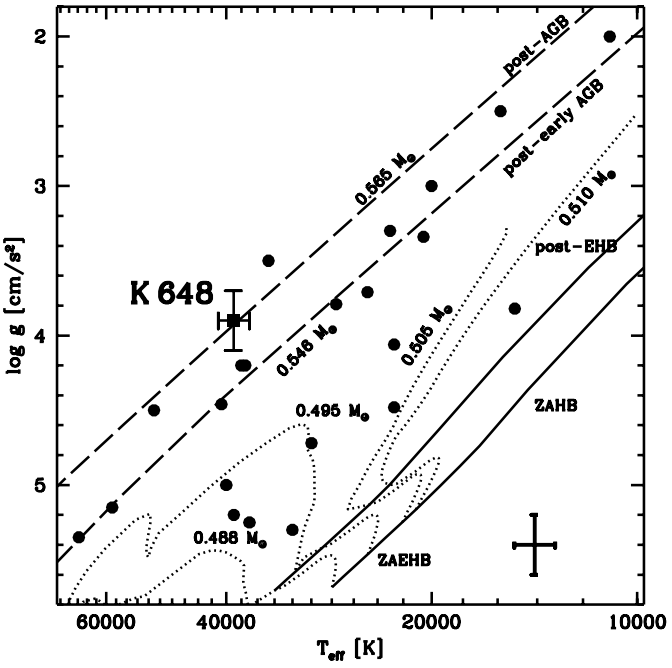

Fig. 12. Position of K 648 in the $\log T_{\rm eff}$–$\log g$ plane compared to theoretical evolutionary tracks of post-AGB hydrogen-burning stars (dashed, masses given in $M_\odot$, Schönberner 1983) and post-EHB evolutionary tracks for [Fe/H] = −1.48 (Dorman et al. 1993). The positions of other UV-bright stars in globular clusters (cf. Moehler et al. 1998, Fig. 3) are marked. The cross in the lower right part indicates the typical errors.

In order to further improve the analysis and the abundance determinations, high-resolution and high-S/N spectra with high spatial resolution (minimize the contamination by the nebula) are highly desirable: such spectra which cover the complete UV range (many lines of different elements and different ionization stages → improvement of $T_{\rm eff}$, cf. Rauch 1993) will separate the possible interstellar and photospheric lines, e.g. in N V $\lambda\lambda\,1238, 1242$ Å. Moreover, we can identify Si IV $\lambda\lambda\,1393, 1402$ Å and S V $\lambda\,1502$ Å in the available FOS spectra at a low S/N ratio which hampers a reliable analysis. Better spectra allow a precise abundance determination of these elements. The optical wavelength range (down to the Balmer edge → improvement of g) gives additional constraints.

Acknowledgements. This research was supported by the DLR under grant 50 OR 9705 5 (Tübingen) and 50 OR 9602 9-ZA (Bamberg). Computations were carried out on CRAY computers of the Rechenzentrum der Universität Kiel, Germany. This research has made use of the SIMBAD Astronomical Database, operated at CDS, Strasbourg, France, of the ST-ECF spectra database, and of the NIST Atomic Spectra Database.

Table 2. Parameters of K 648. The errors are estimated by the variation of $T_{\rm eff}$, $\log g$ and the abundance ratios within their error limits in order to achieve a fit of the synthetic spectrum to the observation. The solar abundance ratios are given by Holweger (1979) and Stürenburg & Holweger (1990). The cluster metallicity is $\frac{1}{178}$ times solar (Harris 1996).

$T_{\rm eff}$/kK	39.0	± 2.0	
$\log(g/\frac{\rm cm}{\rm s^2})$	3.9	± 0.2	solar value
$n_{\rm He}/n_{\rm H}$	8×10^{-2}	± 0.3 dex	1×10^{-1}
$n_{\rm C}/n_{\rm H}$	1×10^{-3}	± 0.3 dex	4×10^{-4}
$n_{\rm N}/n_{\rm H}$	1×10^{-6}	± 0.5 dex	1×10^{-4}
$n_{\rm O}/n_{\rm H}$	1×10^{-3}	± 0.5 dex	7×10^{-4}
$M/M_\odot$	0.57	$^{+0.02}_{-0.01}$	
$L/L_\odot$	3 810	± 1200	
d/kpc	11.1	$^{+2.4}_{-2.9}$	
$t_{\rm post-AGB}$/a	6 800	$^{+3\,500}_{-2\,100}$	
$t_{\rm dyn(PN)}$/a	3 925	$^{+830}_{-1036}$	

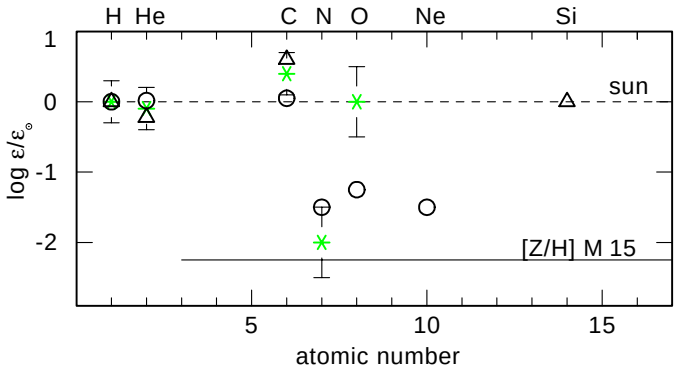

Fig. 13. Photospheric abundances of K 648 (∗: this work, △: Bianchi et al. 2001) and its PN (○: Adams et al. 1984) relative to the sun. The metalicities of the sun and of M 15 are indicated.

References

Adams, S., Seaton, M. J., Howarth, I. D., Aurière, M., & Walsh, J. R. 1984, MNRAS, 207, 471

Alves, D. R., Bond, H., & Livio, M. 2000, AJ, 120, 2044

Bianchi, L., Ford, H., Bohlin, R., Paresce, F., & DeMarchi, G. 1995, A&A, 301, 537

Bianchi, L., Bohlin, R., Catanzaro, G., Ford, H., & Manchado, A. 2001, AJ, 122, 1538

Blöcker, T., & Schönberner, D. 1990, A&A, 240, L11

Dorman, B., Rood, R. T., & O'Connell, R. W. 1993, ApJ, 419, 596

Groenewegen, M. A.T ., & Lamers, H. J. G. L. M. 1989, A&AS, 79, 359

Haas, S., Dreizler, S., Heber, U., Jeffery, S., & Werner, K. 1996, A&A, 311, 669

Harris, W. E. 1996, AJ, 112, 1487

Heber, U., Hunger, K., Jonas, G., & Kudritzki, R. P. 1984, A&A, 130, 119

Heber, U., Dreizler, S., & Werner, K. 1993, Acta Astron. 43, 337

Holweger, H. 1979, Les Éléments et leurs Isotopes dans l'Univers, Université de Liège, Inst., d'Astrophysique, 117

Joy, A. H. 1949, AJ, 110, 424

Küstner, W. 1921, Veröff. d. Univ. Sternwarte zu Bonn, 15

Kurucz, R. L. 1996, IAU Symp., 176 (Kluwer, Dordrecht), 52

McCarthy, J. K., Méndez, R., Becker, S., Butler, K., & Kudritzki, R.-P. 1997, in Planetary Nebulae, ed. H. J. Habing, & H. J. G. L. M. Lamers, IAU Symp. 180 (Kluwer), 122

Moehler, S., Landsmann, W., & Napiwotzki, R. 1998, A&A, 335, 510

Pease, F. G. 1928, PASP, 40, 342

Rauch, T. 1993, A&A, 276, 171

Rauch, T. 1997, A&A, 320, 237

Rauch, T. 2000, A&A, 356, 665

Schneider, S. E., Terzian, Y., Purgathofer, A., & Perinotto, M. 1983, ApJS, 52, 399

Schönberner, D. 1983, ApJ, 272, 708

Stürenburg, S., & Holweger, H. 1990, A&A, 237, 125

Werner, K. 1986, A&A, 161, 177